Inorganic Chemistry

ARTICLE

pubs.acs.org/IC

Existence of Two Concomitant Magnetic Structures Below $T_{Néel}$ for the Natrochalcite, $NaFe^{II}_2(H_3O_2)(MoO_4)_2$

Wassim Maalej,[†,‡] Serge Vilminot,[*,†] Gilles André,[§] Zakaria Elaoud,[‡] Tahar Mhiri,[‡] and Mohamedally Kurmoo[*,∥]

[†]Département de Chimie des Matériaux Inorganiques, IPCMS, UMR 7504 (CNRS-UDS), Université de Strasbourg, 23 rue du Loess, BP 43, 67034 Strasbourg Cedex 02, France

[‡]Laboratoire de l'Etat Solide, Faculté des Sciences, Université Sfax, route de Skoura km 3,5, BP 1171 - 3000 Sfax, Tunisia

[§]Laboratoire Léon Brillouin, CEA-CNRS, CEA Saclay, 91191 Gif-sur-Yvette, France

[∥]Laboratoire DECOMET, CNRS-UMR 7177, Université de Strasbourg, CS 90032, 4 rue Blaise Pascal, 67081 Strasbourg Cedex 1, France

Supporting Information

ABSTRACT: A comparative study of the magnetic properties and magnetic structures of the natrochalcite, $NaFe_2(D_3O_2)(MoO_4)_2$ (**FeD**) to those of the isostructural $NaCo_2(D_3O_2)(MoO_4)_2$ (**CoD**) and $NaNi_2(D_3O_2)(MoO_4)_2$ (**NiD**) is presented. The structural change is a shrinking of the unit cell in the order of the ionic radii of the transition metal, **FeD** > **CoD** > **NiD**. While **NiD** and **CoD** are canted-antiferromagnets with T_N = 28 and 21 K, respectively, **FeD** is an anisotropic 2D-Ising antiferromagnet (T_N = 17 K) with a spin-flop field of 14 kOe at 2 K and the presence of a hysteresis loop reaching only $^1/_4$ of the saturation magnetization in 70 kOe. The critical field decreases almost linearly on warming to T_N. The neutron diffraction patterns of **FeD** below T_N display numerous magnetic Bragg peaks which cannot be assigned to any one magnetic structure but fits well to two superposed sets, one with a temperature independent line width and has a propagation vector $k_1 = (0, 0, 0)$ while for the other there is a clear dependence and $k_2 = (0, 0, {}^1/_2)$. In the $k_1 = (0, 0, 0)$ magnetic structure the moments are parallel to each other within one chain and lie along the *a*-axis but are antiparallel to those in neighboring chains. In contrast **CoD** and **NiD**, for which $k = (0, 0, 0)$, have their moments aligned along the *b*-axis and *ac*-plane, respectively. The second magnetic structure, $k_2 = (0, 0, {}^1/_2)$, is characterized by four sublattices, two per layer, where the moments are in the *ab*-plane and canted with a resultant along the *a*-axis which is compensated by those of the adjacent layers. For the $k_2 = (0, 0, {}^1/_2)$ structure, the scattering coherent length decreases, and the moments tend progressively toward the *a*-axis upon increasing temperature. The coexistence of two concomitant magnetic structures is unprecedented for compounds containing transition metal moment carriers.

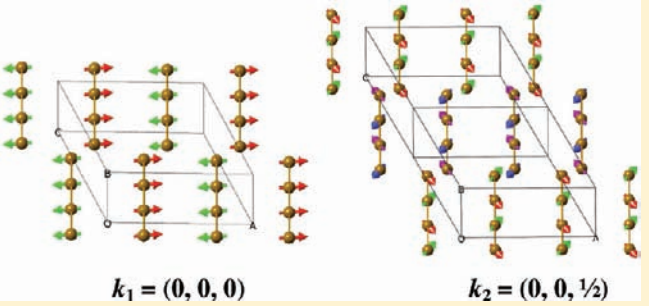

1. INTRODUCTION

One of the wished tasks of magnetochemists is the determination of the magnetic structures of their synthesized compounds in the magnetically ordered state using neutron diffraction.[1] In many cases, this is limited to materials where the number of hydrogen atoms is few compared to the moment carriers or the hydrogen atoms in the materials can be replaced by deuterium.[2] Because of the difficulties in executing the latter requirement when organic ligands are present as well as the large cost and the large quantity required, the number of studies on the metal—organic magnetic materials is limited.[3] However, working with purely inorganic compounds this is less of a problem and is one of the reasons that more magnetic structures are determined for oxides and minerals.[4] For most materials studied, the determined magnetic structure is the same at all temperatures below the long-range magnetic ordering (LRO) temperature. In some cases, there may be additional short-range ordering (SRO) which can be present in both the LRO and paramagnetic temperature regions.[5] Occasionally, the magnetic structures may change with temperature as a consequence of the change in anisotropy or structure. In very rare cases, one can observe the concomitant presence of two ordered magnetic structures where the compounds contain rare-earth moment carriers.[6] We have experienced several of the above cases in our studies on synthetic minerals obtained by hydrothermal technique in the laboratory.[7−10] Here, we present the one rare exception where two concomitant magnetic structures coexist at all temperatures below the Néel transition in a very anisotropic antiferromagnet containing a transition metal moment carrier, $NaFe_2(H_3O_2)(MoO_4)_2$.[11]

By using alkali metal ions, divalent transition metal cations of the first row for their octahedral coordination, and tetrahedral

Received: July 19, 2011
Published: August 03, 2011

anions TO_4, where T is S, Se, or Mo, we and other scientists have synthesized a wide variety of materials.[7−17] While many have natural equivalents, such as Antlerite, Brochantite, or Natrochalcite,[12] there are several that are not known in nature. The selection of high purity starting materials results in transition metal pure materials, which are highly suitable for the study of their magnetic properties unlike the naturally occurred minerals that often contain mixtures of several cations.[7−10] Furthermore, by working in heavy water it is possible to replace the hydrogen atoms in the structures by deuterium, thus providing excellent samples for studies by neutron diffraction.[15]

These studies have revealed a number of different magnetic structures depending on the nuclear structures evidently but unexpectedly not only on the electronic properties of the transition metals but also on the alkali metals and the tetrahedral anions. For example, the sulfate analogue of Antlerite, $Cu_3(OH)_4SO_4$, has a propagation vector $k = (0, 0, 0)$ magnetic structure but that of the selenate analogue is incommensurate with the nuclear lattice, $k = (k_x, 0, 0)$ where $k_x \sim {}^1/_7$ and the moments follow a cycloid.[7] Both have an idle spin for the copper atom at the center of the trimeric unit. The other set for which a wider range of structures have been observed is that belonging to the natrochalcite structure based on $NaCu_2(H_3O_2)(SO_4)_2$.[10−17] All the components in this structure are potentially replaceable, for example, Na by K, Rb, Cs, Tl, Ag, NH_4; Cu by Mn, Fe, Co, Ni, and S by Se, Mo.[10−17] Previous studies on the molybdate series, $NaM_2(H_3O_2)(MoO_4)_2$, M = Co or Ni, reveal collinear antiferromagnetic $k = (0, 0, 0)$ structures for both with the moments along the *b*-axis for Co and along the *ac*-plane for Ni.[10] However, for the $KM_2(H_3O_2)(MoO_4)_2$, M = Mn, Fe, or Co, only the former two exhibit antiferromagnetic ordering and $k = ({}^1/_2, 0, {}^1/_2)$ structures with antiparallel alignment of moments along different directions within the edge-sharing chains. The cobalt complex is paramagnetic at all temperatures above 1.6 K.[17]

To complement these studies as well as to understand the unusual alkali-metal dependence, we have studied the third member of the first series, $NaFe^{II}_2(H_3O_2)(MoO_4)_2$. First to our surprise, the crystals were easily synthesized in good yield and also without contamination with magnetic iron oxides. Thus it provides a very clean study of the magnetism and the magnetic structure determination. The magnetic susceptibility is described as an anisotropic 2D-Ising antiferromagnet, and analysis of the neutron diffraction data reveals the concomitant presence of two magnetic structures. Here, we present these results and also some observations that require further studies, such as the presence of hysteresis loop, and the nonconventional phase diagram where the critical field is linear in temperature.

2. EXPERIMENTAL SECTION

Synthesis. **FeH** was prepared by hydrothermal treatment of a suspension obtained by mixing an iron sulfate solution, $FeSO_4 \cdot 7H_2O$ (1.85 g, 6.65 mmol) in 20 mL of water to a sodium molybdate solution, $Na_2MoO_4 \cdot 2H_2O$ (4.84 g, 20 mmol in 20 mL of water). Boiled and degassed distilled water was used to reduce iron(II) oxidation. The suspension was poured into a PTFE-lined stainless steel pressure vessel (fill factor 1/3) and heated at 210 °C for 24 h. The resultant small red crystals were retrieved by filtration, washed with water, alcohol, and acetone before drying at 40 °C. Energy dispersive X-ray (EDX) analyses confirm the expected formula: % found (% Calc.) Fe 22.41 (22.81), Mo 39.29 (39.19), and Na 4.84 (4.70) which is close to the Na/Fe/Mo = 1:2:2 ratio. The compound for neutron diffraction **FeD** was prepared according to the same process by using D_2O instead of H_2O. Substitution of D for H in the compounds reduces the effect of the high incoherent scattering factor of hydrogen, which gives rise to an increase in the background that can degrade the analyses.

Table 1. Summary of the Single-Crystal X-ray Data for FeH at 173 K[a]

formula	$Mo_2H_3O_{10}NaFe_2$
	$NaFe_2(H_3O_2)(MoO_4)_2$
formula weight	489.6
a (Å)	9.4863(13)
b (Å)	6.3903(8)
c (Å)	7.6386(8)
β (deg)	116.008(3)
V (Å^3)	416.16(9)
Z	2
system	monoclinic
space group	*C*2/*m*
F (000)	460
$D_{calcd.}$ (g.cm^{-3})	3.907(2)
radiation, λ (Å)	Mo Kα_1, 0.71073
μ (mm^{-1})	6.451
hkl range	$-12 < h < 12$, $-8 < k < 7$, $-9 < l < 10$
θ range (deg)	2.97−27.71
total number of reflections	2319
unique reflections	544
unique $I > 2\sigma(I)$	468
R_{int}	0.0285
R_F (all data)	0.0276
wR2 (F_o^2) (all data)	0.0385
GoF	1.071
$\Delta\rho$ e/Å^3 min, max.	−0.679, 0.531

[a] Single crystal **CoH** at 173 K: *a* = 9.3557(9), *b* = 6.3269(6), *c* = 7.6248(7) Å, β = 115.784(2)°, *V* = 406.40(7) Å^3.[10]

Characterizations. Infrared spectra were recorded by transmission through a KBr pellet containing 1% of the crystals using a Digilab Excalibur Series FTIR spectrometer. Analyses by thermogravimetry and differential thermal analysis (TG-DTA) were performed on a TA-SDT-Q600 apparatus under air or argon at a heating rate of 5 °C/min in a platinum crucible. Powder X-ray diffraction (XRD) patterns were recorded using a D8 Bruker diffractometer (Cu Kα_1, 1.5406 Å), equipped with a front monochromator. EDX analyses were made using a Kevex unit of a Jeol 6700 F SEM apparatus. Magnetization measurements were performed in the temperature range 2−300 K and field up to 50 kOe by means of a Quantum Design MPMS-XL SQUID magnetometer. Alternating current (ac) susceptibilities were measured using the same apparatus. Isothermal magnetization at various temperatures were measured using a Quantum design S-VSM magnetometer in field of ±70 kOe on a sample set in PMMA to prevent motion of the crystals in the applied field.

X-ray Crystal Structure Determination. Single crystal XRD data were collected on a Nonius Kappa CCD diffractometer using monochromatized Mo Kα_1 radiation. A small diamond shaped crystal (Supporting Information, Figure S1) was mounted on a glass fiber and cooled by a N_2 stream for data collection at 173 K. The structure was solved by direct methods with SHELXS-97 and refined using SHELXL-97.[18] The final refinement included anisotropic displacement parameters for all non-hydrogen atoms and isotropic ones for hydrogen atoms. Additional details are given in Table 1. Table 2 gives the final atomic positions, and Table 3 the corresponding bond lengths and

dx.doi.org/10.1021/ic2015308 |*Inorg. Chem.* 2011, 50, 9191–9199

Table 2. Fractional Coordinates of the Atoms for FeH from Single-Crystal X-ray Data

atom	x/a	y/b	z/c	U_{eq} or U_{iso} (Å^2)
Fe	0.25	0.25	0.0	0.00640(15)
Mo	0.08226(4)	0.0	0.28891(5)	0.00561(11)
Na	0.0	0.5	0.5	0.0123(5)
OH	0.3511(4)	0.0	0.9156(4)	0.0104(7)
O1	0.7635(3)	0.0	0.4805(4)	0.0118(7)
O2	0.4656(2)	0.7242(3)	0.2602(3)	0.0100(5)
O3	0.8309(4)	0.0	0.8811(4)	0.0097(6)
H1	0.320(6)	0.0	0.805(8)	0.020[a]
H2	0.553(11)	0.0	0.022(19)	0.020[a]

[a] U_{iso} not refined for H atoms.

Table 3. Bond Distances (Å) and Angles (deg) for FeH from Single-Crystal X-ray Data

atoms	distance (Å)	atoms	angle (deg)
	Fe Environment		
Fe−OH	2.105(2) ×2	OH−Fe−OH	180.0
Fe−O3	2.139(2) ×2	OH−Fe−O3	98.06(10) ×2
Fe−O2	2.143(2) ×2	OH−Fe−O3	81.94(10) ×2
⟨Fe−O⟩	2.129	OH−Fe−O2	87.99(10) ×2
		OH−Fe−O2	92.01(10) ×2
		O3−Fe−O3	180.0
		O3−Fe−O2	87.84(10) ×2
		O3−Fe−O2	92.16(10) ×2
		O2−Fe−O2	180.0
	Mo Environment		
Mo−O1	1.727(3)	O1−Mo−O2	109.38(9) ×2
Mo−O2	1.764(2) ×2	O1−Mo−O3	106.35 (14)
Mo−O3	1.818(3)	O2−Mo−O2	108.58(14)
⟨Mo−O⟩	1.768	O2−Mo−O3	111.56(9) ×2
	Na Environment		
Na−O2	2.459(2) ×4	O2−Na−O2	180.0 ×2
Na−O1	2.568(3) ×2	O2−Na−O2	88.40(10) ×2
⟨Na−O⟩	2.495	O2−Na−O2	91.60(10) ×2
		O2−Na−O1	103.20(7) ×4
		O2−Na−O1	76.80(7) ×4
		O1−Na−O1	180.0
	Hydrogen Bonding		
H1−OH	0.76(6)	OH−H1···O1	179(5)
H1···O1	1.97(6)	H1−OH−H2	109(10)
H2−OH	0.82(9)	H1−OH−H2′	116(15)
H1−H2	1.34(11)	OH−H2−OH′	174(7)
H1−H2′	2.10(10)		
H2−OH′	1.72(9)		
OH···OH′	2.539(5)		
H2−H2′	0.91(14)		

angles. Further details of the crystal structure investigation may be obtained from the cif file which has been deposited at the Fachinformationzentrum Karlsruhe, 76344 Eggenstein-Leopoldshafen, Germany, on quoting the depository number CSD-422939 (it can be requested by e-mail from crysdata@fiz-karlsruhe.de).

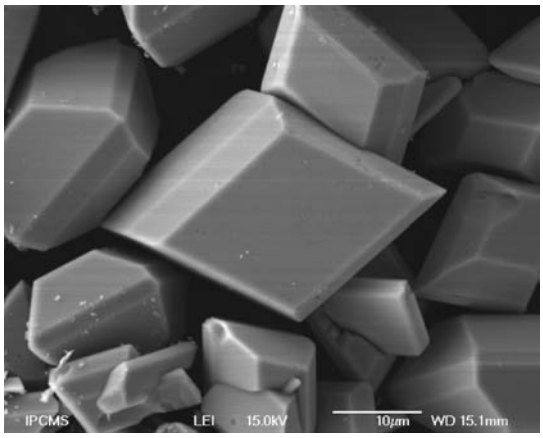

Figure 1. SEM picture of **FeH** crystals.

Magnetic Structure Determination. The neutron diffraction experiments were performed on a powdered sample of the deuterated compound **FeD** at the Laboratoire Léon Brillouin (CEA Saclay) using the multidetector (800 cells) G4.1 (λ = 2.4226 Å) diffractometer for the determination of the magnetic structure and the thermal evolution of the low temperature patterns. Thirteen diffraction patterns were recorded in the 2θ range 5°−84.9° at different temperatures between 1.5 and 25 K. The powder sample was set in a cylindrical vanadium can and held in a liquid helium cryostat. Nuclear and magnetic structures were refined using the FULLPROF program.[19] The nuclear scattering lengths (b_{Na} = 0.3630 × 10^{-12} cm, b_{Fe} = 0.9450 × 10^{-12} cm, b_{Mo} = 0.6715 × 10^{-12} cm, b_O = 0.5803 × 10^{-12} cm, b_D = 0.6671 × 10^{-12} cm, b_H = −0.3739 × 10^{-12} cm) and iron(II) magnetic form factors were those included in this program.

3. RESULTS AND DISCUSSION

Synthesis. Mixing the iron sulfate and alkali molybdate solutions results in an immediate precipitation of a brown powder whose XRD reveals the presence of only two broad lines and thus, do not allow one to identify the compound. The hydrothermal treatment is therefore necessary to crystallize the compound sought. Formation of a basic molybdate without addition of any alkali hydroxide is related to the highly basic character of the alkali molybdate solutions. The reaction yield is around 93% of very small red crystals (Figure 1). Their habit is characteristic of the **CoD** natrochalcite. We note that the samples were not at all contaminated with iron oxides, which is usually the case when working at high temperature in basic media.[20] When additional NaOH was added to the reaction, heavy contamination of the compound with iron oxides was observed. Our method of preparation is more direct than that reported which used a mixture of $Na_2MoO_4 \cdot 2H_2O$, $Na_4Fe(CN)_6 \cdot 10H_2O$, $Na_2C_2O_4$ adjusted to a pH of 10 with NaOH. This method is very likely to oxidize the Fe(II) resulting in only 12% yield.[11] The green color of their crystals may originate from slight contamination of Fe(III) giving intervalence charge transfer bands in addition to the red color of a pure sample.

Crystal Structure. Structures of natrochalcite-type have already been reported using either X-ray or neutron diffraction data,[10−16] and therefore we will restrict this description by highlighting the pertinent information needed for the discussion of the magnetic properties and magnetic structures that will follow. Furthermore, we also discuss the attempt to resolve the

dx.doi.org/10.1021/ic2015308 |Inorg. Chem. 2011, 50, 9191–9199

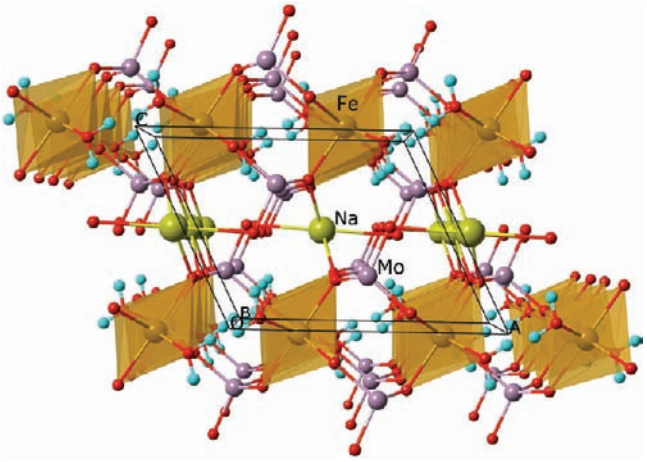

Figure 2. Projection of the crystal structure showing the iron (brown) chains bridged by the H_3O_2 (O red and H cyan), MoO_4 (Mo light purple) and sodium (yellow). Note that the H2 is shown split in two 50% occupied positions.

position of the hydrogen atoms in the H_3O_2 group given that the crystal determination was of high quality ($R < 3\%$) and all the heavy atoms have full occupancy expected in the tables.

The structure (Figure 2) consists of chains of edge-shared FeO_6 octahedra running along the *b*-axis. The Fe−Fe distance is 3.195 Å and Fe−O−Fe angles are 98.8° (OH) and 96.6° (O3), providing the primary magnetic exchange pathway. These values lie on the borderline between antiferromagnetic and ferromagnetic interactions between nearest neighbor moment carriers. The FeO_6 octahedron is distorted with Fe−OH being shorter at 2.105 Å than Fe−O2 and Fe−O3 at 2.141(2) Å; thus a 4 + 2 Jahn−Teller like distortion exists. One can therefore consider the orbital energy to be in the order $d_{xy} < d_{xz}$, $d_{yz} < d_{x^2-y^2} < d_{z^2}$. Furthermore, the octahedron appears to have a trigonal compression giving O−Fe−O angles deviating by ±8° from 90°. The chains are connected by three kinds of three-atom bridges involving H_3O_2 and MoO_4, giving rise to layers parallel to *ab* and NaO_6 connecting the layers in a 3D network. The three connections are secondary magnetic pathways between four magnetic centers of adjacent chains. The MoO_4 tetrahedron is slightly distorted with Mo−O distances very close to the ones observed in **CoH**. The NaO_6 octahedron is also distorted with Na−O bond lengths slightly longer than for **CoH**.[10]

Concerning the H_3O_2 group, refinements involving either a position split around a center of symmetry for the H2 atom or H2 located on this center of symmetry yield very similar results as far as factors of merit are concerned. Whatever the position of the H2 atom, the hydrogen bond through this atom is strong since the OH···OH distance is 2.539(5), that is, much shorter than the sum of the van der Waals radii, 3.04 Å. The OH−H···OH′ bond is nearly linear with an angle of 174° as expected for this kind of hydrogen bond.

Powder XRD. Because of the presence of two concomitant magnetic structures (see later), we had to establish that the sample contains a single crystalline phase. The XRD on a bulk sample of the deuterated compound **FeD** was therefore recorded at room temperature (Supporting Information, Figure S2). The pattern shows very sharp Bragg reflections indicating the highly crystalline nature of the compound, where all the lines were indexed with the natrochalcite structure having the following parameters, space group *C*2/*m*, $a = 9.5072(2)$, $b = 6.4081(1)$, $c = 7.6541(2)$ Å, $\beta = 116.020(1)°$, $V = 419.05(1)$ Å^3. These values are in good agreement with those found by single-crystal diffraction. Furthermore, the background is particularly flat as expected from a well-crystallized sample without any indication of amorphous phases.

Thermal Analyses. The TGA trace for **FeH** under air (Supporting Information, Figure S3) reveals the presence of a first weight loss between 290 and 330 °C associated with an endotherm maximizing at 323 °C. It has been attributed to the departure of one water molecule, $\Delta P/P_{th} = 3.68\%$, $\Delta P/P_{obs} = 3.31\%$. Such a behavior is unique for the iron compound and has not been observed for cobalt and nickel natrochalcite compounds where the departure of the H_3O_2 group as $1.5H_2O$ is more usual, $\Delta P/P_{th} = 5.50\%$. To explain this difference, we can consider that oxidation of iron accompanies the departure of water. After a plateau up to 420 °C, a weight increase is observed up to around 590 °C. The weight increase corresponds to around half an oxygen atom. The endotherm at 650 °C is attributed to an allotropic phase transition of sodium molybdate. A second weight loss starts at around 750 °C and expands up to 1200 °C, the limiting temperature of the apparatus. Under argon, the TGA trace (Supporting Information, Figure S4) has a similar shape with a smaller weight increase compared to the analysis in air. The small oxygen content in the argon cylinder may be responsible for the observed effect.

XRD on a sample previously annealed at 360 °C, that is, during the plateau after water departure, reveals the presence of only three diffraction lines, at $d = 3.3917$, 3.2937, and 3.1821 Å, that could be attributed to the α and β allotropes of $FeMoO_4$.[21] However, with only three lines, no definite conclusion can be drawn. After annealing at 600 °C, the sample is well crystallized, and the XRD pattern is characteristic of the presence of Na_2MoO_4, $Fe_2(MoO_4)_3$, and α-Fe_2O_3.[22] Weight loss calculated according to the following reaction,

$$2NaFe_2H_3O_2(MoO_4)_2 + O_2 \rightarrow Na_2MoO_4 + Fe_2(MoO_4)_3 + Fe_2O_3 + 3H_2O$$

gives a calculated weight loss of 2.26% in agreement with the observed value of 2.3%.

Infrared Spectroscopy. Comparison of the infrared spectra (Supporting Information, Figure S5) of **FeH** and **FeD** allows one to distinguish between the OH(D) and MoO_4 vibration bands. The shift between OH and OD stretching vibration bands at 3426 (2538) and 3196 (2362) cm^{-1} agrees with the expected ratio of $(18/(17 \times 2))^{1/2}$. The H−O−H bending mode is evidenced at 1634 cm^{-1}. Three sharp bands at 916, 855, and 802 cm^{-1}, not shifted between H and D, are attributed to vibrations of the MoO_4 group.[23] According to Nakamoto,[24] the ν_1 and ν_3 bands are observed around 897 and 837 cm^{-1}, respectively. ν_1 is not IR active for a regular tetrahedron but becomes active for a distorted one. The distortion also explains the splitting of the ν_3 vibration band. The bands at 534 and 420 cm^{-1} could be attributed to Fe−O vibrations.

Magnetic Properties. The direct current (dc) magnetic susceptibility was measured on cooling a randomly oriented polycrystalline sample in a field of 100 Oe, and the ac susceptibilities below 50 K were recorded in zero dc field using an ac field of 1 Oe oscillating at 17 Hz (Figure 3a). In the paramagnetic region, the susceptibility follows the Curie−Weiss law, $\chi = C/(T - \theta)$ with $C = 7.86(1)$ emu K/mol and $\theta = -24.7(3)$ K for a

dx.doi.org/10.1021/ic2015308 |*Inorg. Chem.* 2011, 50, 9191–9199

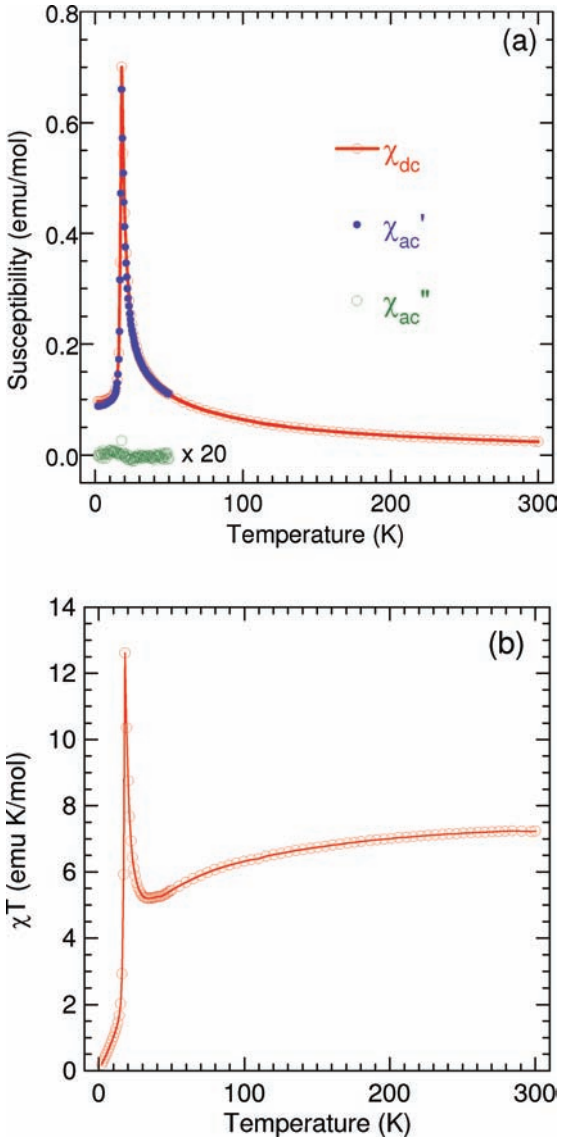

Figure 3. Temperature dependence of (a) the ac- and dc- magnetic susceptibilities and (b) the product of temperature and the dc susceptibility.

fit in the range 100−300 K. The negative value of the Weiss constant is related to a dominant antiferromagnetic interaction above 100 K. From the Curie constant value, we can calculate the effective moment $\mu_{eff} = (8C)^{1/2} = 5.62\ \mu_B$ which is a bit high compared to the expected 4.9 μ_B suggesting an average Landé g-value higher than that of the free electron and is estimated to $g = (8C/S(S+1))^{1/2} = 2.30$. This agrees with those observed for Fe^{II} (d^6, $S = 2$, $L = 2$) in its fundamental state, and it originates from orbital contribution.[25]

The sharp peak in the low temperature susceptibility data suggests a long-range antiferromagnetic ordering of the moments at 17 K. However, the ratio ($^1/_7$) of the value at the lowest temperature to that at the peak is much lower than the $^2/_3$ expected for a statistically random oriented sample of an isotropic antiferromagnet. This is an indication of the anisotropy in the g-values. The plot of χT versus temperature (Figure 3b) reveals another unexpected behavior of an antiferromagnet because of the presence of a minimum, which is more common for ferrimagnets. This anomaly is due to the presence of a ferromagnetic interaction that is weaker than the antiferromagnetic one operating at high temperatures within the plane as indicated by the Curie−Weiss fit. Weak coupling between the layers will result in the long-range 3D ordering. Three interactions can be considered to be the following, between neighboring edge-sharing pair within the chain along the *b*-axis via Fe−O−Fe, between neighboring chains in the *ab*-plane via Fe−O−Mo−O−Fe and Fe−O−H−O−Fe, and between the layers along the *c*-axis via Fe−O−Na−O−Fe. We will discuss the hierarchy of these three interactions in the magnetic structures section.

The real part of the ac susceptibilities (Figure 3a) has a good correspondence with that of the dc susceptibility around the transition temperature while the imaginary part is clearly zero. This indicates that the transition is clearly antiferromagnetic with full compensation of the moments. It also indicates a linear field independence of the susceptibility between 1 and 100 Oe.

The isothermal field dependence magnetization at 2 K (Figure 4a) after zero-field-cooling from 50 K on a sample blocked in PMMA, to prevent motion of the crystals, exhibits a linear dependence until 14 kOe and then there is a sharp deviation to a curved progressive increase to nearly 2 μ_B at 70 kOe, which is only $^1/_4$ of the expected saturation moment for parallel alignment. Following the initial magnetization the full isothermal magnetization displays a skewed hysteresis loop with a coercive field of 4.8 kOe and remanent magnetization of 0.22 μ_B. The sharp deviation from linearity (Figure 4b, Supporting Information, Figure S6) may be considered as a metamagnetic or spin-flop transition.[26] The lower than the expected saturation magnetization of 8 μ_B may be due to the large magnetocrystalline anisotropy as indicated by the susceptibility data discussed above. The $M-T$ phase diagram appears to be linear with field (Figure 4c). We note that on increasing the temperature the critical field is lowered, but linearly, and the magnetization in 70 kOe increases to a maximum at 16 K (Figure 4d), suggesting it gets easier to align the moments at high temperatures. There is a further anomaly which is the initial magnetization being outside the hysteresis loop, like that observed for the unusual metamagnets $Co_2(OH)_2$terephthalate and Co_2(pyromellitate).[27,28] Unlike the latter two compounds where the magnetization in the high field is higher when the sample is field cooled in 50 kOe, for **FeH** the magnetization at 70 kOe after cooling in 70 kOe is only marginally higher than that after zero-field cooled (Figure 4d). This observation suggests that the magnetocrystalline anisotropy is very large indeed to overcome the force of 70 kOe. As such the transition at 14 kOe may be associated with a spin-flop transition. This conclusion is also justified by the susceptibility measurements on cooling in applied higher fields (Supporting Information, Figure S7), where the susceptibility does not tend to saturation as expected for a metamagnetic transition.[25−28] Measurements on single crystal will be required to shed more light on this particular problem. Presently, the present size of the crystals is too small to allow for this type of measurements.

Magnetic Structure. To get more insight into the magnetic behavior, we have proceeded to neutron powder diffraction measurements to determine the magnetic structure for $T < T_N$. The 25 K neutron diffraction pattern was first used to refine the nuclear structure of **FeD**. The refinements allow us to confirm the natrochalcite structure for **FeD**. These parameters were then fixed before proceeding to refine the magnetic structures at 1.6 K. In the final refinement cycles all the parameters were allowed to vary. Table 4 summarizes the corresponding results.

dx.doi.org/10.1021/ic2015308 |*Inorg. Chem.* 2011, 50, 9191–9199

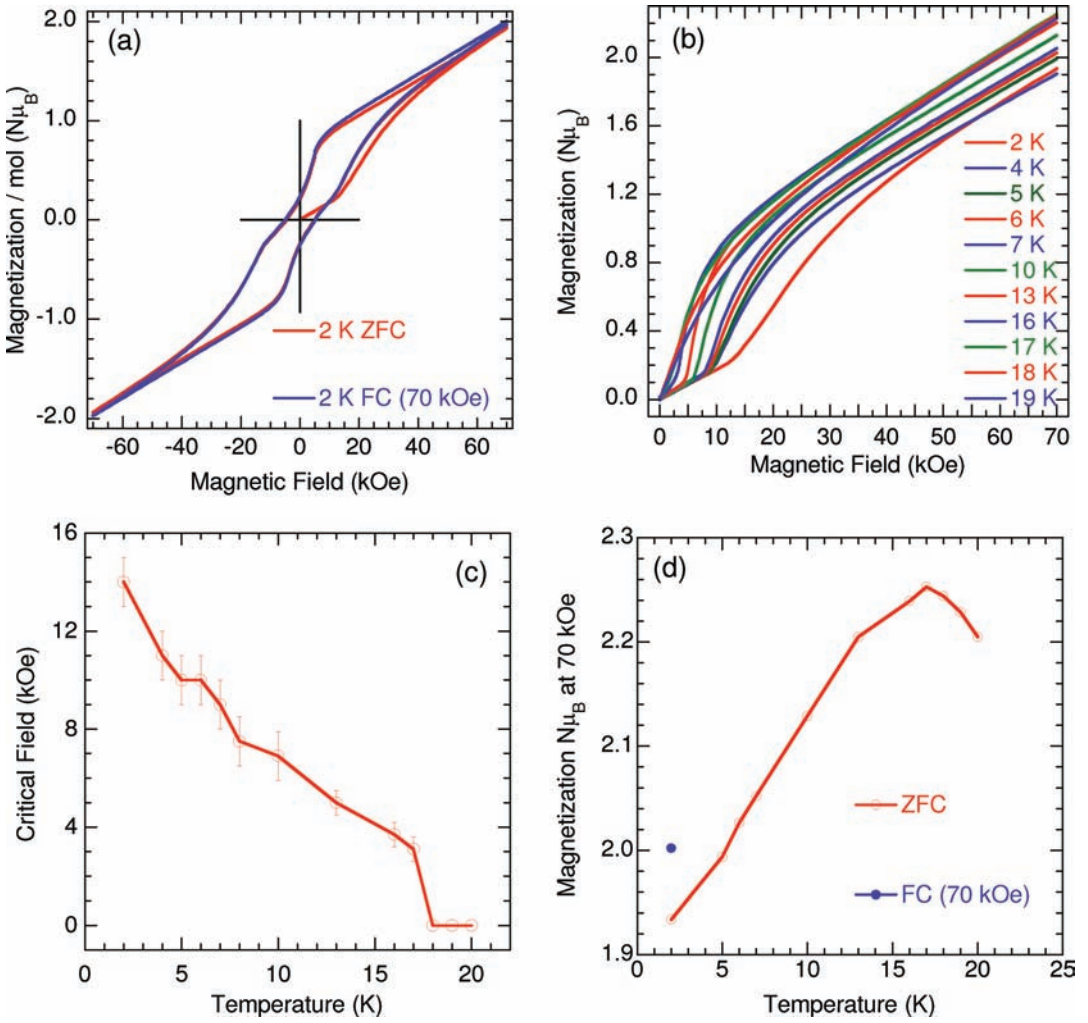

Figure 4. (a) Field dependence of the magnetization after ZFC and FC in 70 kOe; (b) the virgin magnetization after ZFC at different temperatures; (c) the temperature of the critical field, and (d) the temperature dependence of the magnetization at 70 kOe.

Table 4. Summary of the Neutron Powder Data Refinement for FeD at 1.6 K

system	monoclinic
space group	$C2/m$ (No. 12)
a (Å)	9.4896(5)
b (Å)	6.3673(3)
c (Å)	7.6327(4)
β (deg)	116.030(2)
V (Å^3)	414.41(3)
Z	2
2θ range/step	5.0−84.9/0.1
reflections (nuclear/magnetic)	45/306/153
R_p (%)	10.1
R_{wp} (%)	10.5
R_B (%)	2.25
R_F (%)	2.16
R_{mag1} (%)	4.51
R_{mag2} (%)	6.53

The comparison of the neutron diffraction patterns recorded at 1.6 and 25 K (Figure 5) reveals the appearance of numerous new lines at 1.6 K at 2θ values as high as 60°. These lines are of magnetic origin. It is also observed that some of these lines can be indexed with the unit cell parameters of the natrochalcite structure at 25 K. They correspond to lines normally forbidden for space group $C2/m$, that is, lines with $h + k = 2n + 1$ and define a propagation vector $k_1 = (0, 0, 0)$. The other lines being not indexed, a second propagation vector has to be searched, and we find $k_2 = (0, 0, {}^1/_2)$. It is also important to note that the two sets differ in linewidths, being temperature independent for the former and temperature dependent for the latter (Figure 6). These results mean that we have the concomitant presence of two magnetic structures, one with a simple unit cell (SC and k_1), and the other with a double unit cell (DC and k_2).

Moreover, it appears that the integrated intensities and the linewidths of the double cell magnetic peaks do not follow the usual temperature evolution (Figure 6). The intensity of the (-101) line (SC) decreases up to T_N. On the other hand, the intensity of the $(000)^{\pm}$ (DC) line increases above 8 K, reaches a maximum at 15 K, and then decreases. The $(-111)^-$ and $(-111)^+$ lines (double cell) have an intermediate evolution. However, all lines, SC and DC, vanish at the same temperature of 17 K of T_N, in agreement with the magnetic measurements.

dx.doi.org/10.1021/ic2015308 |*Inorg. Chem.* 2011, 50, 9191–9199

Both magnetic structures have been determined using the irreducible representations calculated with the Basireps program according to Bertaut's group theory.[29,30] Table 5 summarizes the corresponding results, and Figure 7 represents the observed and calculated profiles at T = 1.6 K. The presence of only one unique iron site means that it carries the moment from both magnetic structures. Given that the experiment was performed on a randomly oriented powder sample, it is not possible to get information about the presence of domain or other distribution within the unit cell.

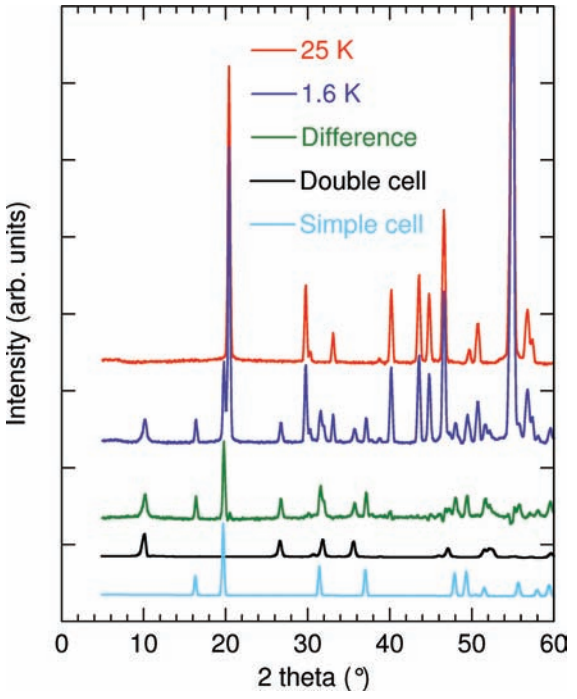

Figure 5. Neutron powder diffraction patterns of **FeD** recorded at 1.6 K (blue) and 25 K (red) on the G4.1 diffractometer and the difference between 1.6 and 25 K patterns (green). The lower traces are the calculated patterns for the two magnetic structures k_1 = (0, 0, 0) in cyan and k_2 = (0, 0, $^1/_2$) in black.

For both cases, antiferromagnetic (AF) ordering with fully compensated moments is observed (Figure 8), and magnetic moment lying within the *ab* plane for the double cell and within the *ac* plane for the simple one. The corresponding resultant moments, 2.61(4) and 2.93(3) μ_B, are close to each other, and their geometrical sum $M = [M_{(SC)}{}^2 + M_{(DC)}{}^2]^{1/2}$ has a value, 3.92(5) μ_B, very close to the expected one for Fe^{2+} of 4 μ_B (Figure 9). The temperature dependence of the total moment follows quite well a law with a critical exponent of 0.125 (Figure 10). One may consider that the system behaves as a 2D-Ising antiferromagnet. As shown in Figure 8, the magnetic structure for the simple cell can be described as ferromagnetic chains of FeO_6 octahedra that are AF coupled forming the two sublattices within the layers parallel to the *ab* plane. Between the successive layers, the coupling is antiferromagnetic. For the double cell, there are 4 sublattices evidenced by arrows with different colors. Within the chains of FeO_6 octahedra and

Table 5. Atomic Positions and Components of the Magnetic Moments for the Two Structures of FeD; k_1 = (0, 0, 0) (top) and k_2 = (0, 0, $^1/_2$) (bottom) at 1.6 K

atom	x/a	y/b	z/c	M_x (μ_B)	M_z (μ_B)	M (μ_B)
			k_1 = (0, 0, 0)			
Fe11	$^1/_4$	$^1/_4$	0	3.09(3)	0.41(3)	2.93(3)
Fe12	$^3/_4$	$^1/_4$	0	−3.09(3)	−0.41(3)	2.93(3)
Fe13	$^3/_4$	$^3/_4$	0	−3.09(3)	−0.41(3)	2.93(3)
Fe14	$^1/_4$	$^3/_4$	0	3.09(3)	0.41(3)	2.93(3)
atom	x/a	y/b	z/c	M_x (μ_B)	M_y (μ_B)	M (μ_B)
			k_2 = (0, 0, $^1/_2$)			
Fe11	$^1/_4$	$^1/_4$	0	0.83(2)	2.48(4)	2.61(4)
Fe12	$^3/_4$	$^1/_4$	0	0.83(2)	−2.48(4)	2.61(4)
Fe13	$^3/_4$	$^3/_4$	0	0.83(2)	2.48(4)	2.61(4)
Fe14	$^1/_4$	$^3/_4$	0	0.83(2)	−2.48(4)	2.61(4)
Fe21	$^1/_4$	$^1/_4$	$^1/_2$	−0.83(2)	−2.48(4)	2.61(4)
Fe22	$^3/_4$	$^1/_4$	$^1/_2$	−0.83(2)	2.48(4)	2.61(4)
Fe23	$^3/_4$	$^3/_4$	$^1/_2$	−0.83(2)	−2.48(4)	2.61(4)
Fe24	$^1/_4$	$^3/_4$	$^1/_2$	−0.83(2)	2.48(4)	2.61(4)

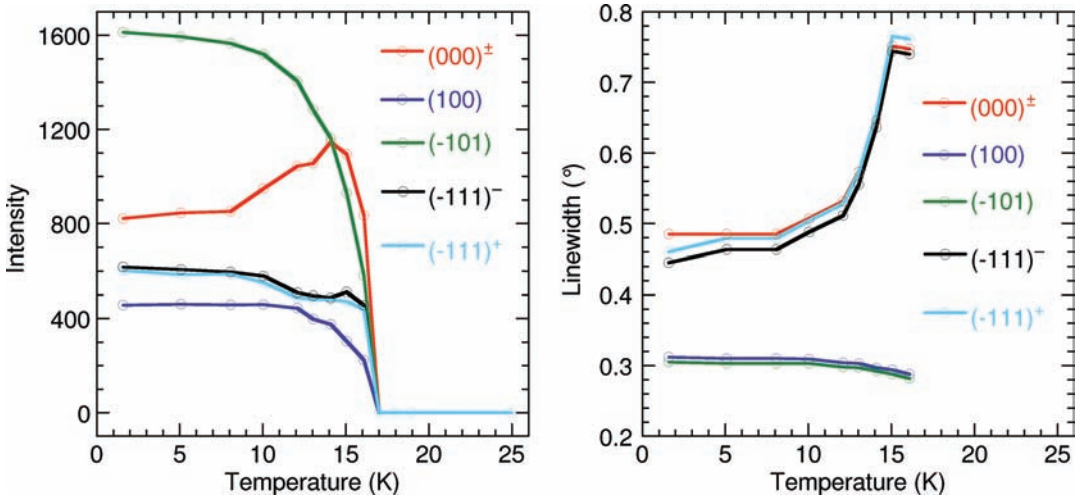

Figure 6. Thermal evolution of the integrated intensity and their linewidths at half-height of lines related to Simple Cell and Double Cell structures: SC (100), 16.35°, blue; SC (−101), 19.73°, green; DC $(000)^{\pm}$, 10.13°, red; DC $(-111)^{-}$, 26.65°, black; and DC $(-111)^{+}$, 35.60°, cyan.

dx.doi.org/10.1021/ic2015308 |*Inorg. Chem.* 2011, 50, 9191–9199

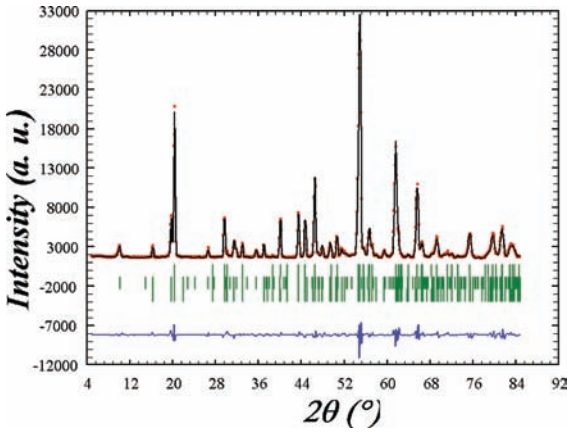

Figure 7. Observed (red) and calculated (black) profiles for **FeD** from refinement of neutron powder diffraction data collected on G4.1 diffractometer (λ = 2.4226 Å) with positions of the reflections (green) in order from top: nuclear, double cell, and simple cell and the difference between observed and calculated profiles (blue).

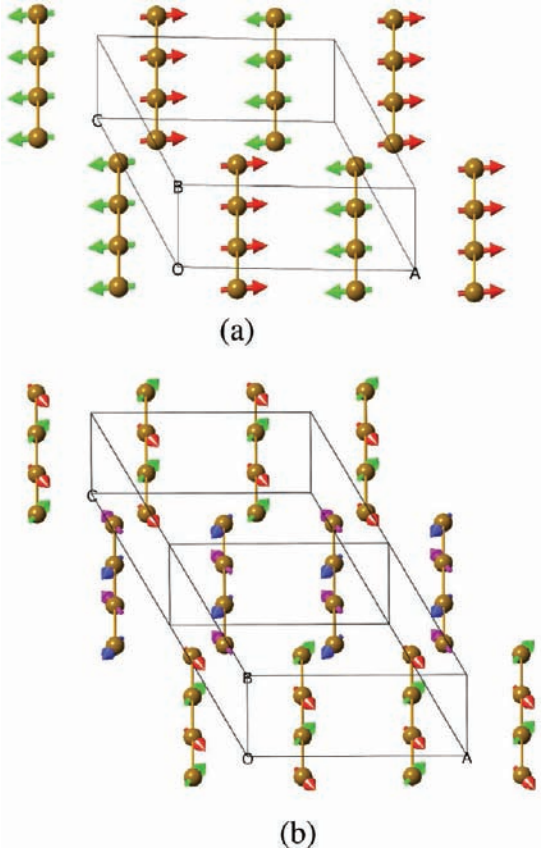

Figure 8. Magnetic structures (a) simple cell, k_1 = (0, 0, 0) and (b) double cell, k_2 = (0, 0, $^1/_2$).

between chains of the layers, the moments are canted AF with a resultant along the *a*-axis. Between the layers, the order is AF.

The thermal evolution of the components of the magnetic moments is shown on Figure 9. The evolution of the components for the simple cell has a typical behavior. On the other hand, a peculiar one is observed in the case of the double cell. The

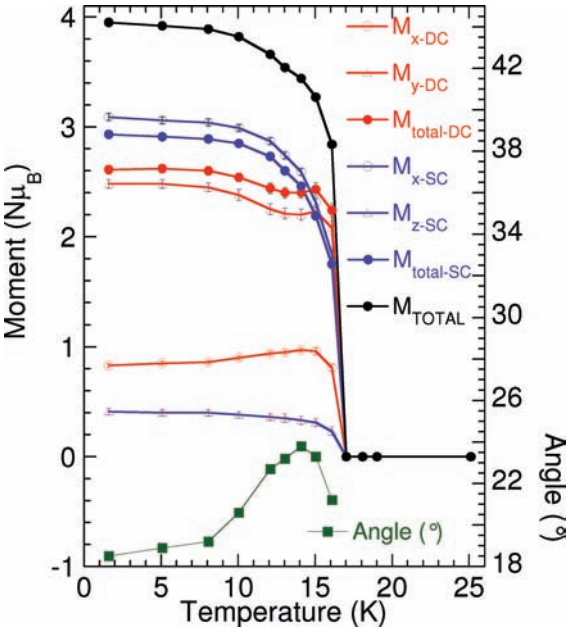

Figure 9. Thermal evolution of the components of the magnetic moments of the simple cell, SC (blue); (b) double cell, DC (red); and the angle (green) between the magnetic moment direction and the *b*- axis in the double cell.

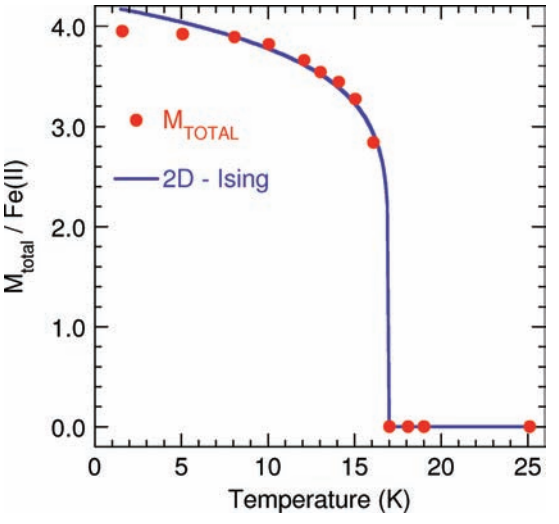

Figure 10. Temperature dependence of the total magnetic moment per iron site (red symbols) superposed with that of the 2D-Ising model (blue line): critical exponent β = 1/8, T_N = 17 K and M_0 = 4.22 μ_B.

evolution of components follows the one observed for the intensities of the magnetic lines. This is related to the fact that the orientation of the moment turns progressively in the *ab* plane on warming the sample to T_N.

4. CONCLUSION

The most unexpected result of this study is the presence of two concomitant ordered magnetic structures {k_1 = (0, 0, 0) and k_2 = (0, 0, $^1/_2$)} below the Néel transition at 17 K in a transition metal containing magnet, $NaFe_2(D_3O_2)(MoO_4)_2$ whereas the cobalt and nickel analogues exhibit a single collinear one {k_1 =

dx.doi.org/10.1021/ic2015308 |*Inorg. Chem.* 2011, 50, 9191–9199

(0, 0, 0)}. While electronic factors are the principal elements in determining the direction of the moments, the present findings suggest that the exchange through the non-magnetic components, such as Na and K on the one hand or SeO_4 and MoO_4 on the other, may have dramatic consequence on the nature of the resulting magnetic structures in this particular series. It is also to be noted that the local anisotropy of the transition metals cannot be ignored. While the observation is unique to our best knowledge in the studies of transition metal minerals, other observations, such as the presence of the hysteresis loop and the linear dependence of the critical field (spin-flop), remain to be clarified for a full comprehension of this anisotropic 2D-Ising antiferromagnet.

■ ASSOCIATED CONTENT

Supporting Information. X-ray crystallographic information file in CIF format. Photo of the single crystal used in the XRD data collection. XRD pattern at room temperature. DT-TGA in air and under argon. Infrared spectra. Plot of the derivative of the isothermal magnetization at different temperatures. The susceptibility measured on cooling in different magnetic fields. This material is available free of charge via the Internet at http://pubs.acs.org.

■ AUTHOR INFORMATION

Corresponding Author

*Phone: (33) 3 68 85 13 21 (M.K.). E-mail: vilminot@ipcms.u-strasbg.fr (S.V.), kurmoo@unistra.fr (M.K.).

■ ACKNOWLEDGMENT

This work was supported by the CNRS (France), CEA (France), and the Université de Strasbourg (France). We are grateful to Corinne Bailly and Lydia Brelot of the "Service de Crystallographie, Université de Strasbourg" for the determination of the single crystal structure.

■ REFERENCES

(1) *Powder diffraction, theory and practice*; Dinnebier, R. E., Billinge, S. J. L., Eds.; RSC Publishing: London, England, 2008.

(2) Bacon, G. E. *Neutron diffraction*; Clarendon Press: Oxford, England, 1962.

(3) Schweitzer, J. *J. Phys. IV France* **2003**, 103.

(4) See for example the Neutron facilities annual reports: (a) http://www.ill.eu/fileadmin/users_files/Annual_Report/, (b) http://www-llb.cea.fr/fr-en/activ08-09/ (c) http://www.isis.stfc.ac.uk/about-isis/annual-report/, (d) http://www.ncnr.nist.gov/AnnualReport/.

(5) Ben Salah, M.; Vilminot, S.; André, G.; Richard-Plouet, M.; Bourée-Vigneron, F.; Mhiri, T.; Kurmoo, M. *Chem.—Eur. J.* **2004**, *10*, 2048.

(6) (a) André, G.; Boureé, F.; Kolenda, M.; Lesniewska, B.; Oles, A.; Szytula, A. *Phys. B* **2000**, *292*, 176. (b) Sniadecki, Z.; Idzikowski, B.; Greneche, J.-M.; Kerschl, P.; Rössler, U. K.; Schultz, L. *J. Phys.: Condens. Matter* **2008**, *20*, 425212. (c) Durivault, L.; Bourée, F.; Chevalier, B.; André, G.; Weill, F.; Etourneau, J.; Martinez-Samper, P.; Rodrigo, J. G.; Suderow, H.; Vieira, S. *J. Phys.: Condens. Matter* **2003**, *15*, 77. (d) Kuznietz, M.; André, G.; Bourée, F.; Pinto, H.; Ettedgui, H.; Melamud, M. *Phys. Rev. B* **1994**, *50*, 3822. (e) Prokes, K.; Munoz-Sandoval, E.; Chinchure, A. D.; Mydosh, J. A. *Phys. Rev. B* **2008**, *78*, 014425. (f) Reehuis, M.; Zeppenfeld, K.; Jeitschko, W.; Stüsser, N.; Ouladdiaf, B.; Loidl, A. *J. Magn. Magn. Mater.* **2002**, *251*, 260.

(7) Vilminot, S.; André, G.; Bourée-Vigneron, F.; Richard-Plouet, M.; Kurmoo, M. *Inorg. Chem.* **2007**, *46*, 10079.

(8) Vilminot, S.; André, G.; Richard-Plouet, M.; Bourée-Vigneron, F.; Kurmoo, M. *Inorg. Chem.* **2006**, *45*, 10938.

(9) (a) Ben Salah, M.; Vilminot, S.; André, G.; Bourée-Vigneron, F.; Richard-Plouet, M.; Mhiri, T.; Kurmoo, M. *Chem. Mater.* **2005**, *17*, 2612. (b) Vilminot, S.; Richard-Plouet, M.; André, G.; Swierczynski, D.; Bourée-Vigneron, F.; Kurmoo, M. *Inorg. Chem.* **2003**, *42*, 6859.

(10) Vilminot, S.; André, G.; Bourée-Vigneron, F.; Baker, P. J.; Blundell, S. J.; Kurmoo, M. *J. Am. Chem. Soc.* **2008**, *130*, 13490.

(11) Chu, D.-Q.; Pan, C.-L.; Duan, L.-M.; Xu, J.-Q.; Wang, L.-M.; Yu, J.-H.; Wang, T.-G. *Inorg. Chem. Commun.* **2002**, *5*, 989.

(12) (a) http://www.mindat.org/min-2853.html; (b) Palache, C. *Am. J. Sci.* **1939**, *237*, 451.(c) Palache, C.; Berman, H.; Frondel, C. *The System of Mineralogy of James Dwight Dana and Edward Salisbury Dana*, Yale University, 7th ed.; John Wiley and Sons, Inc.: New York, 1951; Vol. II, p 1837.

(13) (a) Cord, P.-P.; Courtine, P.; Pannetier, G. *C. R. Acad. Sci. Paris, Serie C* **1970**, *270*, 946. (b) Clearfield, A.; Sims, M. 1.; Gopal, R. *Inorg. Chem.* **1976**, *15*, 335. (c) Pezerat, H. *Bull. Soc. Fr. Mineral. Cristallogr.* **1967**, *90*, 549. (d) Tardy, M.; Bregeault, J.-M. *Bull. Soc. Chim. France* **1974**, 1866.(e) Rumanova, I. M.; Volodina G. F. *Doklady Acad. Nauk SSSR*, **1958**, *123*, 78 (in Russian).

(14) (a) Giester, G. *Z. Kristallogr.* **1989**, *187*, 239. (b) Giester, G.; Zemann, J. *Z. Kristallogr.* **1987**, *179*, 431.

(15) (a) Chevrier, G.; Giester, G.; Jarosch, D.; Zemann, J. *Acta Crystallogr.* **1990**, *C46*, 175. (b) Chevrier, G.; Giester, G.; Zemann, J. *Z. Kristallogr.* **1993**, *206*, 7.

(16) (a) Krickl, R.; Wildner, M. *Eur. J. Mineral* **2009**, *21*, 65. (b) Krickl, R.; Wildner, M. *Eur. J. Mineral* **2007**, *19*, 805.

(17) Maalej, W.; Vilminot, S.; André, G.; Damay, F.; Elaoud, Z.; Mhiri, T.; Kurmoo, M. *Inorg. Chem.* **2011**, *50*, 3286.

(18) Sheldrick, G. M. *SHELXL-97*, 2 ed.; University of Göttingen: Göttingen, Germany, 1997.

(19) Rodriguez-Carvajal, J. *FULLPROF, Rietveld, Profile Matching and Integrated Intensity Refinement of X-Ray and/or Neutron Data*, Version 3.5d; Leon-Brillouin Laboratory/CEA: Saclay, France, 2005.

(20) Cornell, R. M.; Schwertmann, U. *The Iron Oxides, Structure, Properties, Reactions, Occurrence and Uses*; VCH Publishers: Weinheim, Germany, 1996.

(21) JCPDS files 22-1115 and 22-628.

(22) JCPFS files 12-773, 30-1195 and 33-664.

(23) Beran, A.; Giester, G.; Libowitzky, E. *Mineral. Petrol.* **1997**, *61*, 223.

(24) Nakamoto, K. *Infrared and Raman Spectra of Inorganic and Coordination Compounds*, 5th ed.; John Wiley & Sons: New York, 1997.

(25) Herpin, A. *Theorie du Magnétisme*; Presses Universitaire de France: Paris, France, 1968.

(26) (a) Blundell, S. J. *Magnetism in Condensed Matter*; Oxford, University Press: Oxford, England, 2001. (b) Marvilliers, A.; Parsons, S.; Riviere, E.; Audiere, J.-P.; Kurmoo, M.; Mallah, T. *Eur. J. Inorg. Chem.* **2001**, *5*, 1287.

(27) Kurmoo, M.; Kumagai, H.; Green, M. A.; Lovett, B. W.; Blundell, S. J.; Ardavan, A.; Singleton, J. *J. Solid State Chem.* **2001**, *159*, 343.

(28) Kumagai, H.; Kepert, C. J.; Kurmoo, M. *Inorg. Chem.* **2002**, *41*, 3410.

(29) Bertaut, E. F. *Acta Crystallogr., Sect. A* **1968**, *24*, 217.

(30) (a) *KAREP — a program for calculating irreducible space group representations*; Hovestreydt, E.; Aroyo, I.; Sattler, S.; Wondratschek, H. *J. Appl. Crystallogr.*, **1992**, *25*, 544; (b) J. Rodriguez-Carvajal *BASIREPS — a program for calculating non-normalized basis functions of the irreducible representations of the little group Gk for atom properties in a crystal*; Laboratoire Léon Brillouin (CEA(CNRS): CEA Saclay, Gif sur Yvette, France, 2004.